ELSEVIER

Journal of Nuclear Materials 300 (2002) 230–236

journal of nuclear materials

www.elsevier.com/locate/jnucmat

In situ electrochemical impedance spectroscopy of Zr–1%Nb under VVER primary circuit conditions

Gabor Nagy [a,*], Zsolt Kerner [a], Tamás Pajkossy [b]

[a] *Department of Physical Chemistry, KFKI Atomic Energy Research Institute, P.O. Box 49, H-1525 Budapest, Hungary*

[b] *Research Laboratory of Materials and Environmental Chemistry, Chemical Research Centre, Hungarian Academy of Sciences, P.O. Box 17, H-1525 Budapest, Hungary*

Received 18 July 2001; accepted 26 October 2001

Abstract

Oxide layers were grown on tubular samples of Zr–1%Nb under conditions simulating those in VVER-type pressurised water reactors, viz. in near-neutral borate solutions in an autoclave at 290 °C. These samples were investigated using electrochemical impedance spectroscopy which was found to be suitable to follow in situ the corrosion process. A $-\mathrm{CPE}_{ox}\|R_{ox}-$ element was used to characterise the oxide layer on Zr–1%Nb. Both the CPE_{ox} coefficient, σ_{ox}, and the parallel resistance, R_{ox}, were found to be thickness dependent. The layer thickness, however, can only be calculated after a calibration procedure. The temperature dependence of the CPE_{ox} element was also found to be anomalous while the temperature dependence of R_{ox} indicates that the oxide layer has semiconductor properties. The relaxation time – defined as $(R_{ox}\sigma_{ox})^{1/\alpha}$ – was found to be quasi-independent of oxidation time and temperature; thus it is characteristic to the oxide layer on Zr–1%Nb. © 2002 Elsevier Science B.V. All rights reserved.

1. Introduction

Since zirconium alloys are essential in nuclear reactor technology, used as fuel cladding, pressure tubes, fuel channels and fuel spacer grid materials, extensive experimental and theoretical investigations are required to understand their corrosion properties in detail for applying more severe operating conditions, longer service time, higher burnups, higher pH in pressurised water reactor (PWR) coolants.

Among the number of techniques applied to study the corrosion processes on zirconium alloys, electrochemical techniques, e.g. open circuit potential measurements (OCP) and electrochemical impedance spectroscopy (EIS), are widely used because they give in situ information on the kinetics of corrosion and on oxide layer thickness. Ample results of EIS are available for the various western type PWR and BWR Zircaloy, cladding materials, however, much less information is available for the VVER (Russian type PWR) cladding material Zr–1%Nb.

Impedance spectroscopy can be applied ex situ on pre-oxidised samples and in situ during oxidation. The first type of measurements is usually performed in acid media at room temperature, whereas the latter is done at high temperatures. The composition of oxidising aqueous media is very similar those of the primary circuit cooling liquids. It has been already demonstrated several times that the corrosion of Zircaloy can be followed by in situ EIS but similar measurements for Zr–1%Nb have not yet been done extensively.

There is no general consensus in the literature about the interpretation of impedance spectra of zirconium alloys, indicating that the analysis of results in terms of equivalent circuits is not straightforward. Wikmark et al. [1] found an $-R_s-[R_1-(R_2\|\mathrm{CPE}_2)]\|\mathrm{CPE}_1-$ equivalent circuit to describe the results of their ex situ

* Corresponding author. Tel.: +36-1 392 2222; fax: +36-1 392 2299.

E-mail address: nagyg@sunserv.kfki.hu (G. Nagy).

0022-3115/02/$ - see front matter © 2002 Elsevier Science B.V. All rights reserved.
PII: S0022-3115(01)00735-8

measurements on different Zircaloys in sulphuric acid solution. R denotes the resistance (R_s is the solution resistance) and CPE is the common abbreviation of a certain type of dispersive capacitor, i.e. the constant phase element with an impedance $Z_{CPE} = (1/\sigma)(i\omega)^{-\alpha}$, where σ is the CPE coefficient, α the CPE exponent, ω the angular frequency and i the imaginary unit. Note that for ideal capacitance $\alpha = 1$. These authors related R_1, R_2, CPE_1, CPE_2 to the dielectric and electron transport properties of the oxide layer.

Göhr et al. [2] described EIS of the non-oxidised Zircaloy-4 in terms of an $-R_s-[Z_F \| Y]-$ circuit where Z_F corresponds to the Faraday process on the surface, the native oxide layer is described by Y, the so-called Young impedance (for details see Ref. [2]). They found a different circuit, $-R_s-[R_d-(R_{ct}\|C)]\|(R_2\|CPE_2)\|CPE_1-$ to be valid for their in situ high-temperature results [3] taking also into account electrochemical reactions by the $[R_d-(R_{ct}\|C)]$ elements; here R_d describes the resistance of the dense layer, C the adsorption, and R_{ct} the charge transfer. The authors related CPE_1 to the oxide as a whole, while $(R_2\|CPE_2)$ was attributed to the porous part of the oxide layer.

Bardwell and McKubke [4] suggested a simple $-R_s-(R_p\|CPE)-$ circuit for their ex situ measurements of pure zirconium in borate buffer solutions. R_p was considered as charge transfer resistance and CPE was related to the oxide layer.

Gebhardt [5] used a much more complicated equivalent circuit $-R_s-(R_4\|C)-R_3\|(R_1-CPE_1)\|(R_2\|CPE_2)\|Y)-$ to describe his measurement on Zircaloy-4 in sulphuric acid solution. The $(R_4\|C)$ term represents the porous oxide layer while the remaining part of the circuit was related to the bulk oxide.

Recent in situ high-temperature measurements of Albinet et al. [6] of Zircaloy-4 were analysed in terms of an $-R_s-(R_1\|CPE_1)-(R_2\|CPE_2)-$ equivalent circuit. The authors related only one of the parallel $R\|CPE$ terms to the oxide layer, the origin of the second term has not yet been assigned: a number of hypotheses, among others the possibility of oxygen diffusion in the oxide, was investigated, but no conclusive solution has been proposed.

A similar picture was obtained by Schefold et al. [7] by monitoring the corrosion layer impedance of pure Zr and Zircaloy-4 in situ at 360 °C. They used two separate $R\|CPE$ terms in series to describe the porous and dense part of the oxide layer, respectively.

The results of our previous ex situ EIS measurements of oxidised Zr–1%Nb in sulphuric acid solution [8] could be adequately described in terms of the $R_s-(CPE\|R_p)$ equivalent circuit, while Krysa [9] recommended a much more complicated circuit $-R_s-R_1\|(R_3-C_2)\|(R_5-C_4)\|C_6-$ to be valid for the same material measured ex situ in potassium sulphate solution. The advantage of this latter circuit is that ideal capacitances are involved only, thus the thickness of the oxide layer, d, can be calculated simply from C_6 by the general equation

$$C = \varepsilon\varepsilon_0 A/d, \quad (1)$$

where ε_0 is the vacuum permittivity, ε is the dielectric constant (relative permittivity) of the oxide layer (usually estimated to be between 20 and 31.5 [10]) and A is the surface area.

A similar approach was used by a number of authors [11,12] calculating oxide thickness values from impedances measured at a single frequency, also taking into account the oxide porosity [13].

However, if the CPE element is used to characterise the dielectric properties of oxide layers, the thickness calculation is not straightforward since CPE has no unequivocal physical interpretation although it is frequently observed when measuring the dielectric response of solid materials [14]. In this case, the thickness cannot be calculated directly from Eq. (1). One can use a calibration procedure measuring samples with known thickness values. This can be done through a direct scaling with the mass data [7] or by applying a normalising frequency [2]. Extrapolating the universal capacitance to high frequencies the infinite frequency capacitance can be obtained [4,6], from which the thickness can readily be calculated. If the CPE exponent is close to one the CPE coefficient may be considered as a pure capacitance [1], and the layer thickness can be calculated directly by Eq. (1).

The CPE behaviour can be attributed to a number of different reasons. It can be of geometric origin, as surface roughness or porosity, as it was extensively investigated by Cox and Wong [15] but it may appear due to an intrinsic dielectric property of the oxide as it is indicated by the temperature dependent measurements of Schefold and co-workers [7].

Furthermore, the above-described analyses of impedance spectra were always based on the assumption that the oxide layer behaves as a dielectric. However, it is well known [14] that semiconductor impedances often behave in a similar way when their impedance is measured. As it was shown by Blackwood [16] the impedance of passivated titanium electrodes is dominated by the space charge layer capacitance of the semiconductor oxide; thus the thickness cannot be directly determined from the measurements. This may be the case, particularly if the donor density is high or the electric field in the layer is small such as under open circuit conditions. Recent photoelectrochemical investigations of Lee et al. [17] have shown that the passive film on Zircaloy-4 is an n-type semiconductor with a band-gap energy of about 3 eV.

The aim of our work was to follow the corrosion of Zr–1%Nb in situ by EIS under conditions similar to those in the primary circuits of VVERs. A particularly

important question is whether the oxide layer behaves as a dielectric or it has semiconductor properties. The results of EIS are expected to provide information about the kinetics and the mechanism of oxide layer growth on Zr–1%Nb.

2. Experimental

Solartron 1286 or Electroflex EF453 potentiostats coupled to a Solarton 1250 frequency response analyser were used for our electrochemical measurements. Impedance spectroscopy was carried out in the frequency range of 64 kHz–0.1 Hz (sometimes 0.001 Hz) with an AC amplitude of 5 mV, cyclic voltammetry was done with 100 mV/s scan rate. The in situ measurements were performed in an autoclave in a two-electrode arrangement daily at 290 °C, and during every heating period at 20, 110, 200 and 290 °C, respectively. The potential difference between the two identical Zr–1%Nb electrodes was set to zero. The ex situ measurements were performed in an ordinary glass electrochemical cell at room temperature, in a normal three-electrode arrangement with Pt counter electrode and saturated calomel reference electrode in the same solution.

Zr–1%Nb tubular samples were cleaned in accordance with the ASTM G2M standard. Two identical samples were placed into a PARR 4532 autoclave connected to electrical feedthroughs. The autoclave was filled with an aqueous solution containing 0.8 g/kg boric acid, 5 mg/kg ammonium hydroxide and 5 mg/kg potassium hydroxide—these being typical concentrations of the primary circuit of a VVER. Analytical grade chemicals and ultrapure water obtained from a REWA clean water system were used. After de-aeration by argon gas the samples were kept in the solution at 290 °C up to 140 days. Periodically, the system was cooled down to room temperature to perform temperature dependent measurements.

3. Results and discussion

From a series of ex situ cyclic voltammetric (CV) and EIS measurements we could conclude that non-oxidised, ‘metallic’ Zr–1%Nb show typical ‘inert metal’ behaviour. The oxidised samples were also proved to be inert. There is a wide potential range where no significant potential dependence of the impedance spectra was found.

We also investigated the effect of dissolved oxygen. No changes were observed in the spectra after deaerating the cell with Ar gas. This indicates that the diffusion of the dissolved oxygen does not play a rate-determining role in our system.

These findings enabled us to perform in situ EIS measurements in a two-electrode arrangement by fixing the potential difference between the two electrodes to zero. The results clearly show that impedance spectroscopy detects the presence of the oxide layer on Zr–1%Nb. While the non-oxidised (metallic) sample has a simple spectrum indicating a single interfacial process, the shape of spectra changes very soon after the start of oxidation as it is shown in Fig. 1. A new peak appears at higher frequencies on the phase angle curve and the low frequency part becomes distorted. As oxidation proceeds the high frequency peak becomes more pronounced.

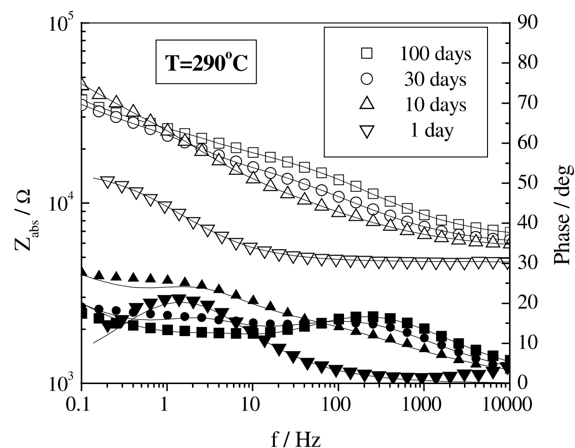

Fig. 1. Time dependence of in situ impedance spectra of Zr–1%Nb at 290 °C (open symbols – magnitude; solid symbols – phase angle). The solid lines show the results of non-linear fits (cf. text).

Additional information can be obtained by measuring temperature dependence of impedance spectra. As is seen in Fig. 2(a) for non-oxidised Zr–1%Nb the changes in the shape of the curves clearly indicate that the interfacial process is temperature dependent. Similarly, the spectra of oxidised Zr–1%Nb (Fig. 2(b)) are also temperature dependent; particularly, the high frequency part changes strongly.

As we already pointed out in the introduction, there is no general consensus in the literature about the interpretation of impedance spectra of zirconium alloys. It is usually assumed that there exists a charge transfer process related to the oxidation and the oxide layer shows dispersive capacitive behaviour coupled to conductive charge transport. To interpret the impedance spectra we fitted various equivalent circuits to the results. The more elements we use in the equivalent circuit the better agreement with the measurements can be obtained. Therefore, it is essential to understand the physical meaning of the fitted parameters.

3.1. Non-oxidised Zr–1%Nb

The spectrum of non-oxidised Zr–1%Nb reflects a single interfacial process, which is conventionally described by the equivalent circuit

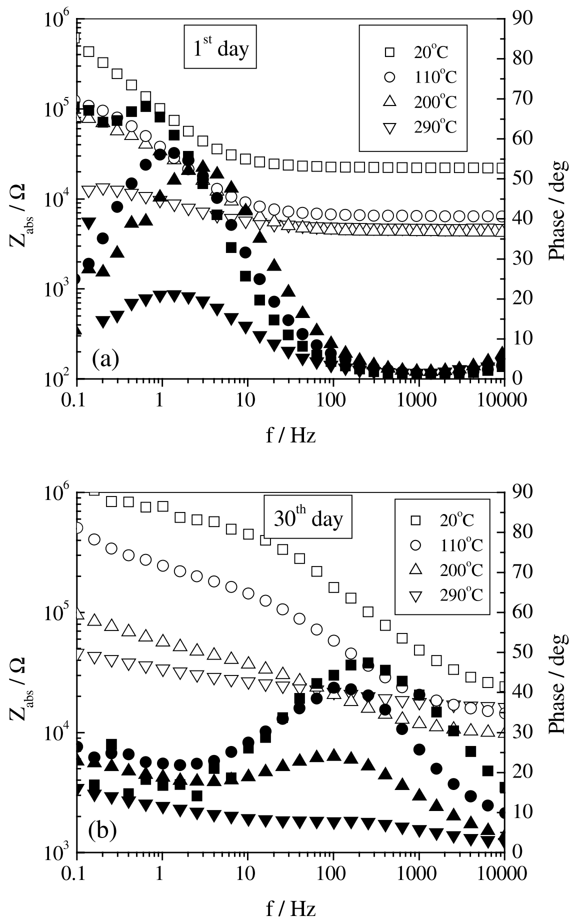

Fig. 2. Temperature dependence of in situ impedance spectra of non-oxidised and oxidised Zr–1%Nb (open symbols – magnitude, solid symbols – phase angle).

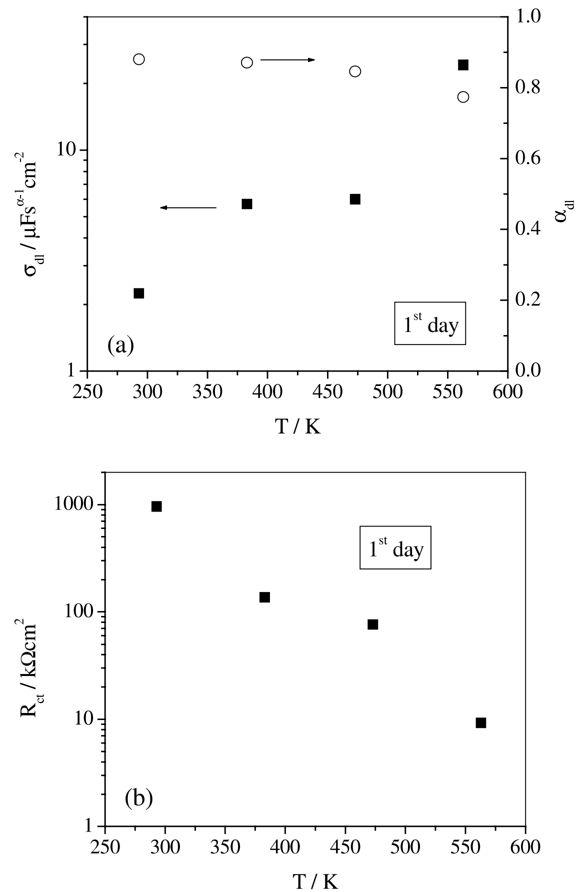

Fig. 3. Temperature dependence of the parameters obtained by fitting the impedance spectra of metallic Zr–1%Nb with the R_s–$CPE_{dl}\|R_{ct}$ equivalent circuit (see. Eq. (2) in text). The CPE coefficient, σ_{dl}, (■) and the CPE exponent, α_{dl}, (○) are shown in (a). R_{ct} (■) is shown in (b).

$$-R_s\text{–}(R_{ct}\|\text{CPE}_{dl})\text{–} \tag{2}$$

if the mass transport in the solution is fast enough. In Eq. (2) R_s denotes the solution resistance, and the interfacial process (presumably oxidation of Zr) is represented by the R_{ct} charge transfer resistance. The double layer capacitance is frequency dependent and is described by the CPE_{dl} element.

It can be seen from Fig. 3(a) and (b) that all of the parameters of equivalent circuit (2) are temperature dependent. The charge transfer resistance R_{ct} (Fig. 3(b)) decreases with increasing temperature as it is expected, since R_{ct} is proportional $1/k$ and this reaction rate coefficient increases with increasing temperature.

The CPE_{dl} coefficient, σ_{dl}, increases with increasing temperature, whereas the CPE_{dl} exponent, α_{dl}, slightly decreases (Fig. 3(a)). It is known that the CPE behaviour may be either of geometrical or physico-chemical origin [18]. Since the geometrical factors, porosity or roughness, are independent of temperature, but kinetic and energetic parameters – as we saw this for R_{ct} – are strongly temperature dependent, we can conclude that there is an inhomogeneity in the chemical properties of the Zr–1%Nb surface and this leads to the CPE behaviour.

The observed temperature dependence of σ_{dl} is in contrast with the expectations. On the one hand, the double layer capacitance, according to the classical electrochemical theories, e.g. the Gouy–Chapman theory, should decrease with increasing temperature. On the other hand, if CPE_{dl} reflects the capacitance of the insulating native oxide layer on non-oxidised Zr–1%Nb, the temperature dependence would be similarly decreasing since the dielectric constant is expected to decrease with increasing temperature (cf. Eq. (1)).

Summarising our findings, we may conclude that EIS reflects a single interfacial process on the non-oxidised

Zr–1%Nb, which is described by the charge transfer resistance. The double layer capacitance is frequency dependent and is described by a CPE element, the temperature dependence of which is anomalous.

3.2. Oxidised Zr–1%Nb

As oxidation proceeds new features appear in the spectra (Fig. 1). We assigned the high frequency part (the new peak on the phase angle diagram) to the presence of the oxide layer. The changes in the low frequency part may be attributed to either a diffusion-limited process (with semi-infinite, or transparent boundary conditions) or a process with long characteristic time. We analysed our results by fitting a number of different equivalent circuits (based on the literature) finding that the spectra are not distinctive enough to enable us to select a unique equivalent circuit that would describe the results much better than any other. The relatively best choice consists of a Randles-circuit ($-R_s-[C\|(R_p-W)]-$) in series with an $R\|$CPE type element. The measured and fitted curves are in reasonable agreement with each other as it is shown by the solid lines in Fig. 1. This circuit represents a physical picture that would be appropriate to our system: the Randles-circuit describes a diffusion-controlled interfacial process and the $R\|$CPE element is characteristic to a large family of dielectric materials (with the inevitable resistance for electron transport through the layer). Unfortunately, we found the fitted parameters to be strongly correlated; therefore we cannot consider this circuit to be the representative one.

Assuming that the high frequency region does reflect the presence of the oxide layer which is considered to be homogeneous [8], we analysed the results only in the 10 Hz–10 kHz frequency range by fitting a simple

$$-R_s-(\mathrm{CPE_{ox}}\|R_{ox})- \tag{3}$$

equivalent circuit. In Eq. (3) R_s is the solution resistance, while $\mathrm{CPE_{ox}}$ and R_{ox} are related to the conductance and the charge storing property of the oxide layer.

The first thing we should mention about the results of fits is that R_s decreases with increasing temperature, which is expected, and we also found that it shows an increasing trend with longer oxidation time, i.e. with increasing layer thickness. Unfortunately, we cannot analyse this finding in detail since our experimental arrangement introduces an unknown resistance of the contacts. Therefore we cannot interpret the increase of R_s as an increasing oxide layer resistance due to the increasing layer thickness.

3.2.1. Oxidation time dependence

By plotting the fitted parameters in Fig. 4(a) and (b) as a function of oxidation time, one can see that the

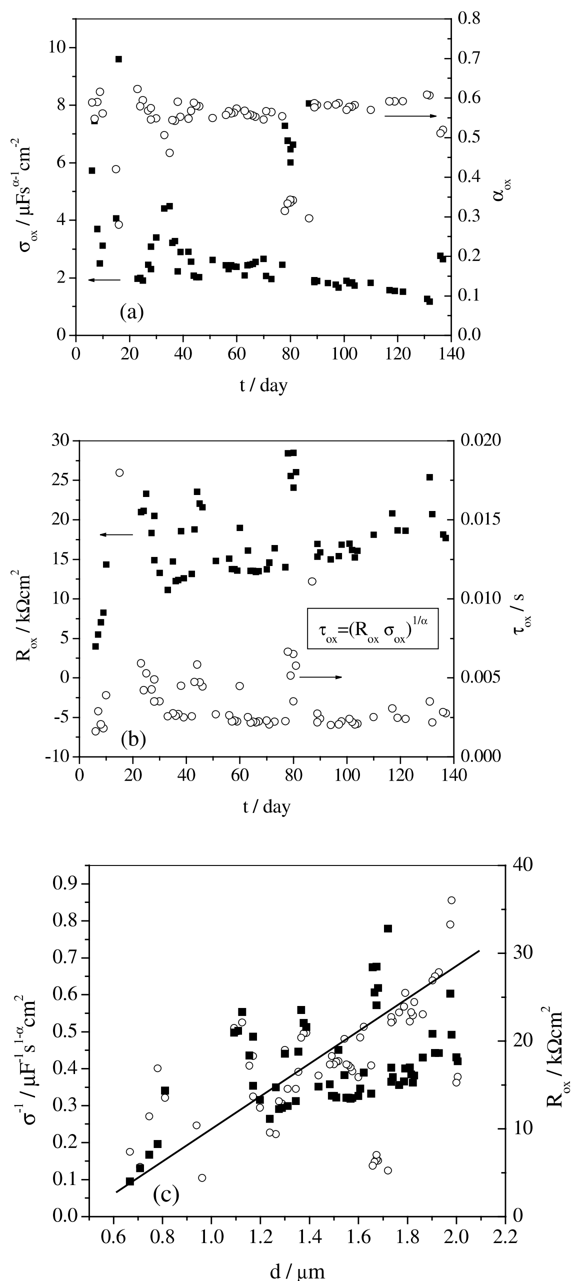

Fig. 4. Time dependence of the parameters obtained by fitting the impedance spectra of Zr–1%Nb measured at 290 °C with the R_s–$\mathrm{CPE_{ox}}\|R_{ox}$ equivalent circuit (see Eq. (3) in text). The CPE coefficient, σ_{ox}, (■) and the CPE exponent, α_{ox} (○) are shown in (a). R_{ox} (■) and the characteristic time, τ_{ox} (○) (see Eq. (4) in text) are shown in (b). The reciprocal of the $\mathrm{CPE_{ox}}$ coefficient, $1/\sigma_{ox}$, and R_{ox} as a function of the layer thickness, d, known from gravimetry (cf. Eq. (5)) are shown in (c). The straight line in (c) is for guide the eye.

$\mathrm{CPE_{ox}}$ coefficient, σ_{ox}, decreases, whereas the $\mathrm{CPE_{ox}}$ exponent, α_{ox}, is constant (Fig. 4(a)). In contrast to this,

the parallel resistance, R_{ox}, increases (Fig. 4(b)). These trends are in accordance with the expectations: the CPE element may reflect the capacitive behaviour of the oxide layer, thus σ_{ox} decreases with increasing layer thickness according to Eq. (1). R_{ox}, reflecting the electrical conductivity of the layer, should increase with increasing thickness. As the $R\|$CPE element may correspond to the charge transport through the oxide layer, we calculated a characteristic relaxation time, τ_{ox}, according to the following equation:

$$\tau_{ox} = (R_{ox}\sigma_{ox})^{1/\alpha}. \quad (4)$$

Fig. 4(b) shows that τ_{ox} is practically independent of oxidation time indicating that after the first couple of days the chemical properties of the oxide layer do not change during corrosion within our time scale. In Fig. 4(c) we relate R_{ox} and CPE_{ox} to the layer thickness; the latter is determined by Eq. (5), established in our previous work [8] in the units of μm and day, as

$$d = 0.39t^{1/3}. \quad (5)$$

We found both σ_{ox}^{-1} and R_{ox} to show an increasing trend as the layer thickness d increases. Although the data points are scattered a linear relationship may be established which is visualised by the straight line in Fig. 4(c). Thus both CPE_{ox} and R_{ox} may be a measure of the oxide layer thickness; they can be used to follow the oxidation of Zr–1%Nb.

3.2.2. Temperature dependence

Further information can be obtained from the temperature dependence of the fitted parameters. As it is shown in Fig. 5(a) the CPE_{ox} coefficient increases unexpectedly with increasing temperature while the CPE_{ox} exponent usually slightly decreases. This trend is similar to those we found for the non-oxidised sample. R_{ox} is found to decrease with increasing temperature (Fig. 5(b)) indicating that the oxide shows semiconductor properties. We may assume, therefore, that the $R\|$CPE term expresses some combination of charge storing and charge transport features with a broad time constant distribution. One possible theory to rationalise this behaviour is the theory of continuous time random walk (CTRW) developed by Scher and Lax [19] which has been successfully applied to describe the stochastic transport of a series of disordered systems, such as semiconductors. The relaxation time, τ_{ox}, may be considered as a characteristic transition rate in this model. Since we could not find a distinct temperature dependence (Fig. 5(b)) for τ_{ox}, it may represent a basic property of the oxide layer.

The results of in situ EIS let us conclude that the R$\|$CPE element characterises the charge transport across the oxide layer on Zr–1%Nb. Both the resistance and the CPE element can be used to follow the oxidation of Zr–1%Nb. Direct calculation of the layer thickness from the parameters, however, is not possible without the knowledge of a scaling factor that can only be obtained from independent measurements.

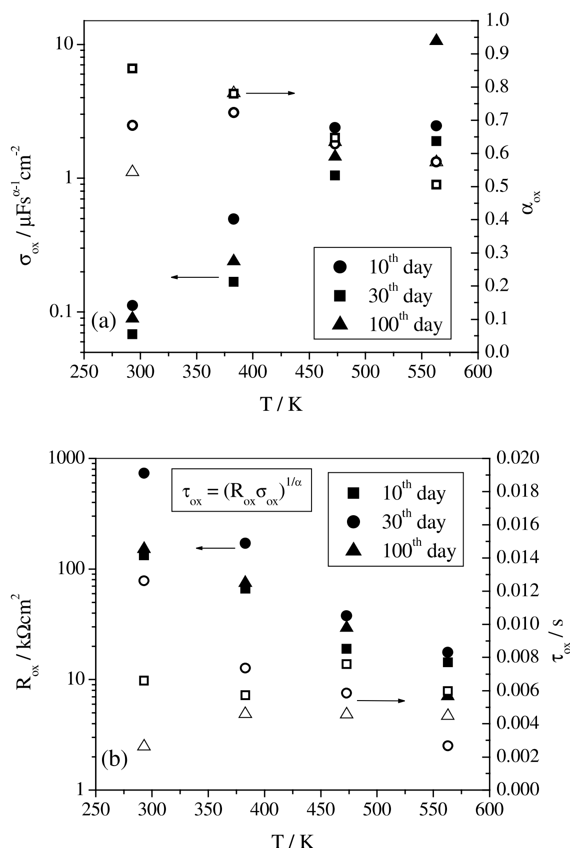

Fig. 5. Temperature dependence of the parameters obtained by fitting the impedance spectra of oxidised Zr–1%Nb with the R_s–$CPE_{ox}\|R_{ox}$ equivalent circuit (see Eq. (3) in text). The CPE coefficient, σ_{ox}, (filled symbols) and the CPE exponent, α_{ox}, (open symbols) are shown in (a). R_{ox} (filled symbols) and the characteristic time, τ_{ox} (open symbols) (see Eq. (4) in text) are shown in (b).

4. Summary

A series of in situ high-temperature EIS measurements was performed to follow the oxidation of Zr–1%Nb under conditions similar to those which prevail in VVER-type PWRs. The spectra of non-oxidised Zr–1%Nb indicate the presence of a single interfacial process with an unexpected temperature dependence of the frequency dependent double layer capacitance. A –$CPE_{ox}\|R_{ox}$– element was used to characterise the oxide layer on Zr–1%Nb. Both the CPE_{ox} coefficient, σ_{ox}, and the parallel resistance, R_{ox}, were found to be thickness

dependent. However, the layer thickness can only be calculated after a calibration procedure. The temperature dependence of the CPE_{ox} element was also found to be anomalous while the temperature dependence of R_{ox} indicates that the oxide layer has semiconductor properties. The relaxation time defined as $(R_{ox}\sigma_{ox})^{1/\alpha}$ was found to be quasi-independent of oxidation time and temperature. Thus it is characteristic of the oxide layer on Zr–1%Nb.

Acknowledgements

We wish to thank Professor Robert Schiller, KFKI AEKI, for helpful discussions. One of the authors (G.N.) is indebted to the Hungarian Academy of Sciences for the Bolyai fellowship. Financial support from the National Foundation for Scientific Research, Hungary under contract no. T029894 is acknowledged.

References

[1] G. Wikmark, P. Rudling, B. Lehtinen, B. Hutchinson, A. Oscarsson, E. Ahlberg, in: E.R. Bradley, G.P. Sabol (Eds.), Zirconium in the Nuclear Industry: Eleventh International Symposium, ASTM STP 1295, ASTM, 1996, p. 55.

[2] H. Göhr, J. Schaller, H. Ruhmann, F. Garzarolli, in: E.R. Bradley, G.P. Sabol (Eds.), Zirconium in the Nuclear Industry: Eleventh International Symposium, ASTM STP 1295, ASTM, 1996, p. 181.

[3] H. Göhr, J. Schaller, C.-A. Schiller, Electrochim. Acta 38 (1993) 1961.

[4] J.A. Bardwell, M.C.H. McKubre, Electrochim. Acta 36 (1991) 647.

[5] O. Gebhardt, J. Nucl. Mater. 203 (1993) 17.

[6] B. Albinet, B. Sala, A. Frichet, H. Takenouti, Seventh International Symposium on Electrochemical Methods in Corrosion Research, EMCR2000, Budapest, Hungary, May 28–June 1, 2000, CD-ROM No. 086.

[7] J. Schefold, D. Lincot, A. Ambard, E. Moleiro, O. Kerrec, Seventh International Symposium on Electrochemical Methods in Corrosion Research, EMCR2000, Budapest, Hungary, May 28–June 1, 2000, CD-ROM No. 058.

[8] G. Nagy, G. Battistig, A. Csordás-Tóth, Z. Kerner, T. Pajkossy, J. Nucl. Mater. 297 (2001) 62.

[9] J. Krysa, ACH Models Chem. 137 (2000) 249.

[10] Waterside corrosion of zirconium alloys in nuclear power plants, IAEA-TECDOC-996, 1998.

[11] N. Ramasubramanian, V.C. Ling, J. Nucl. Mater. 183 (1991) 226.

[12] S.M. Abd El-Motal, N.H. Hilal, W.A. Badawy, Electrochim. Acta 39 (1994) 2611.

[13] B. Cox, J. Nucl. Mater. 148 (1987) 332.

[14] A.K. Jonscher, Dielectric Relaxation in Solids, Chelsea Dielectric, London, UK, 1983.

[15] B. Cox, Y.M. Wong, J. Nucl. Mater. 218 (1995) 324.

[16] D.J. Blackwood, Electrochim. Acta. 46 (2000) 563.

[17] S.J. Lee, E.A. Cho, S.J. Ahn, H.S. Kwon, Electrochim. Acta. 46 (2001) 2605.

[18] T. Pajkossy, J. Electroanal. Chem. 364 (1994) 111.

[19] H. Scher, M. Lax, Phys. Rev. B. 7 (1973) 4491.